

Development of a didactic plant and a human-machine interface to compare different digital controllers

Nelson N. N. Yamaguti* Bruno G. Dutra*
Antonio S. Silveira*

* *Institute of Technology, Federal University of Pará, Belém, 66075-110, Brazil (e-mail: nelson.yamaguti@itec.ufpa.br, brunodutra@ufpa.br, asilveira@ufpa.br).*

Abstract: This article presents a comparison between the effectiveness of controllers strongly consolidated in the classical and modern control theory, for this, several performance indices were used. In order to carry out this research, it was proposed the development of a low cost didactic plant with two inputs and one output, with dynamics similar to those of heavy cargo transport aerial vehicles used in the military area. In addition to the elaboration of the didactic process, this work includes the development of a human-machine interface to control the angular position of the plant in real time. The results show that the construction of the didactic process was performed successfully, because the plant worked as expected, in addition, the responses obtained to the PID, LQR and LQG controllers corresponded satisfactorily.

Keywords: PID; LQR; LQG; Didactic Plant; Human-Machine Interface; Real-Time Control.

1. INTRODUCTION

The history of control systems can be divided into three phases, the first phase corresponding to the first intentional uses of the feedback mechanism during the beginning of the industrial revolution (Friedland, 2012). In World War II (1940), the second phase of control systems began, where several mathematicians, physicists and engineers from that period began to research contents which are now found in literature that address concepts of classical control theory. From this stage of the evolution of control systems, it was possible to study several dynamic behaviors in SISO systems (Single-Input Single-Output). According to Stevens et al. (2016), these systems are described in “black box” by transfer functions (mathematical relationships that constitute an input and output relationship of the process).

In the late 1950s, with the increase in the complexity of systems, where processes started to have multiple inputs and multiple outputs (Multiple-Input Multiple-Output - MIMO), the third phase of control systems began, in this period, studies of modern control theory begin, in which, in this approach, processes are characterized by systems of first-order differential equations coupled and represented in the form of matrices (Friedland, 2012).

According to Misgeld et al. (2013), the interconnection of current systems in industries has presented an increase in complexity in relation to the theory of control and automation, that way, companies such as *National Instruments*®, *WEG*® and *Quanser*® show that there has been an increase in demand in what it concerns the number of companies that develop products in order to provide didactic processes and services to academia and industry.

Thus, the purpose of this work consists in the production of a MISO low cost didactic process (Multiple-Input Single-Output) with two inputs and one output with the purpose of making a comparison between different performance indices between controllers strongly consolidated in classical and modern control theory.

This didactic process has dynamics similar to heavy delivery vehicles in the military aerospace sector, such as the *Boeing CH-47 Chinook*, where propulsion is carried out by means of two propellers (Yip, 1984). In the tests performed in this research, the variable to be controlled is the angular position of the mobile part of the system, that is, the control of this process is similar to the pitch control of these aircraft.

2. PROTOTYPE CONSTRUCTION

2.1 Prototype assembly

To develop the design to make mass production feasible, the prototype was built using professional 3D modeling software for engineering; Among the software available for the production of this project, was chose to use the Computer Aided Design program (CAD) 3D Inventor®. Figure 1 shows the design made using the Inventor® software.

After the modeling presented in Figure 1, the project, which was printed on a 3D printer, is present in Figure 2, in this same figure, it is possible to see other items that were fundamental for the functioning of the didactic process.

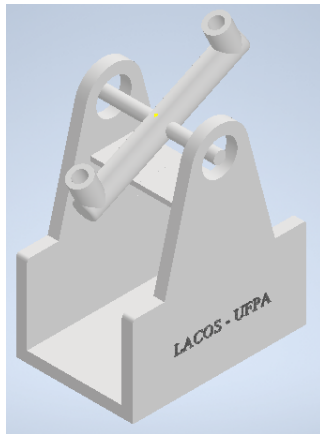


Fig. 1. 3D model.

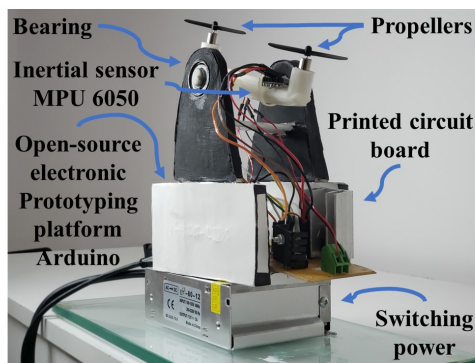


Fig. 2. Process developed for the research.

2.2 Motors drive circuit

The circuit design was produced using Proteus[®] software and the Figure 3 shows the electrical circuit diagram responsible for reading the signal from the MPU-6050 sensor, sending the signal from the control action (signal generated by an arduino UNO output, which it's an open source electronic prototyping platform based on the ATmega328P microcontroller) and power from the external source.

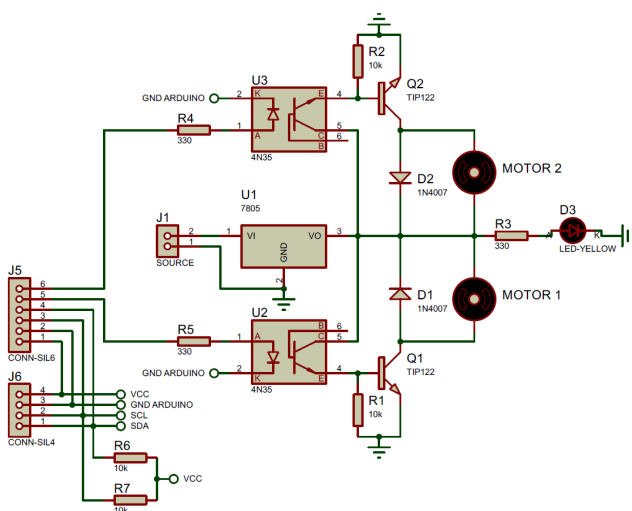


Fig. 3. Motors drive circuit.

In Figure 3, it's observed that the J5 and J6 posts were used to connect the sensor to the aduino, while the resistors R6 and R7 were used in the pull-up configuration to ensure a good reading of the angular position of the didactic process. On the other hand, the R4 and R5 resistors were used to protect the LED inside the optical couplers U2 and U3, which they're used to electrically isolate the control circuit (connected to the aduino) from the drive circuit (connected to the source and to the motors). Subsequently, R1 and R2 resistors were connected in the pull-down configuration and Q1 and Q2 transistors were used as a switching system, followed by D1 and D2 diodes, used in the free-wheel diode configuration. Finally, the R3 resistor was used to protect the D3 LED, which indicates the connection between source and board. As the motors need a supply voltage of 3.2 V and a maximum current of 100 mA, a 12 V voltage source capable of providing a current of 5 A was used.

2.3 Graphic interface

To plot the results, a Human Machine Interface (HMI) was developed, through this HMI, the user enters the controller tuning parameters and the desired angular position (reference), which is selected in real-time through the *Dial* feature (positioned in the center of the upper part of the Figure 4).

Through these feature available in the HMI, it is possible see in Figure 4 that the HMI plots the following curves in real time: measured angle (blue in the upper graph), angle with the desired reference (white in the upper graph), voltage applied to motor 1 (blue in the lower graphic) and motor 2 (red in the lower graphic).

This HMI was made using the software Qt Designer for the development of the design and the software Spyder for the programming of the design in Python language.

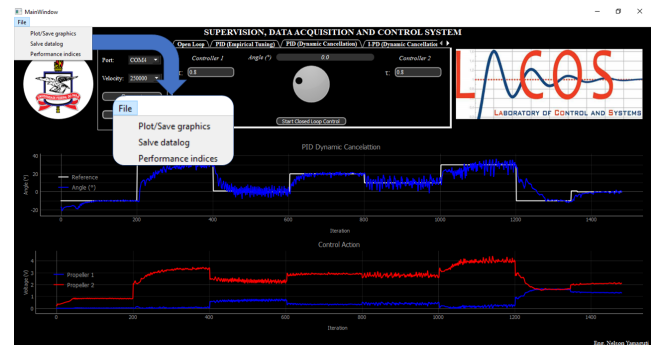


Fig. 4. Example showing the response to a PID controller.

In addition, as indicated in the upper left corner of Figure 4, the HMI has three additional features: one of these features allows the designer to plot and save the curves obtained, in order to analyze the graphics later; the second feature allows the user to save the datalog containing the output signal, inputs and the simulation time vector, to be used or provided to other students, teachers or researchers; and the third feature to show performance indices to facilitate comparison between controllers.

3. IDENTIFICATION VIA NON-RECURSIVE LEAST SQUARES

For practical purposes, the system identification method used, was the application of least squares, in addition, the choice of the order of the system for the application of the Non-Recursive Least Squares (NRLS) estimator was made taking into account two factors: knowledge of the dynamics of the process, and according to the value of the multiple correlation coefficient (R^2), thus, the system was considered to be second order. The value of R^2 is used as a validation index of the estimated model, and can be defined as

$$R^2 = 1 - \frac{\sum_{k=1}^N [y(k) - \hat{y}(k)]^2}{\sum_{k=1}^N [y(k) - \bar{y}]^2} \quad (1)$$

Where k , $y(k)$, $\hat{y}(k)$, \bar{y} and N correspond to discrete time instant, real output value, estimated output, average output and number of samples, respectively. According to Coelho and dos Santos Coelho (2016), for many practical applications, values of R^2 between 0.8 and 1 can be considered sufficient.

3.1 NRLS: A Polynomial Approach

To control the MISO process using classical control theory techniques, the controllers were designed using a strategy to act in a decentralized manner, therefore observing Figure 5 and considering the Auto Regressive model with inputs eXogenous (ARX), as the process has two inputs ($u_1(k)$ and $u_2(k)$: two propulsion engines) and one output ($y(k)$: angular position of the didactic process), it is possible to write the output signal as (2)

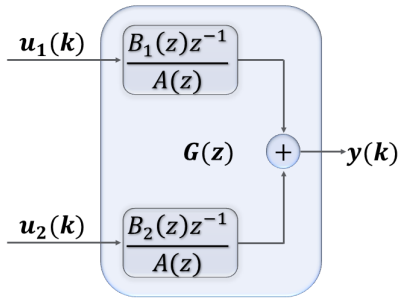


Fig. 5. MISO system block diagram.

$$y(k) = \frac{B_1(z)z^{-1}}{A(z)}u_1(k) + \frac{B_2(z)z^{-1}}{A(z)}u_2(k) \quad (2)$$

Where $B_1(z)$ and $B_2(z)$ are the polynomials of the numerators and $A(z)$ represents the characteristic polynomial of the open loop transfer function. Thus, taking into account that the estimated discrete model is second order, (2) can be represented as a difference equation, as in (3)

$$y(k) = a_1y(k-1) + a_2y(k-2) + b_{10}u_1(k-1) + b_{11}u_1(k-2) + b_{20}u_2(k-1) + b_{21}u_2(k-2) \quad (3)$$

Thus, by means of the (3), it is possible to establish the vector that contains the read data (measures vector - \mathbf{y}),

the matrix that encompasses the input and output data of the system (matrix of regressors - Φ) and the vector of estimated parameters (θ), where:

$$\mathbf{y}^T = [y(0) \ y(1) \ \dots \ y(N)] \quad (4)$$

$$\Phi = \begin{bmatrix} -y(0) & 0 & u_1(0) \\ -y(1) & -y(0) & u_1(1) \\ \vdots & \vdots & \vdots \\ -y(N-1) & -y(N-2) & u_1(N-1) \\ 0 & u_2(0) & 0 \\ u_1(0) & u_2(1) & u_2(0) \\ \vdots & \vdots & \vdots \\ u_1(N-2) & u_2(N-1) & u_2(N-2) \end{bmatrix} \quad (5)$$

$$\theta^T = [a_1 \ a_2 \ b_{10} \ b_{11} \ b_{20} \ b_{21}] \quad (6)$$

After defining (4) and (5), the parameters of (6) can be calculated using (7)

$$\mathbf{y} = \Phi\theta \quad (7)$$

To calculate θ using (7), it will be necessary that Φ is a square matrix, however Φ is a matrix of order $\Phi_{N,6}$. Thus, according to Aguirre (2014), it is necessary to apply the pseudo-inverse matrix. Therefore, the solution of the non-recursive least squares estimator was performed by calculating θ as follows

$$\theta = [\Phi^T\Phi]^{-1}\Phi^T\mathbf{y} \quad (8)$$

The sequence of steps applied at the input of the system, was chosen in such a way as to obtain the best multiple correction coefficient defined in (1). Thus, using the input and output data present in Figure 6, with the sampling period $T_s = 0.0135s$ and determining (8), the result was obtained

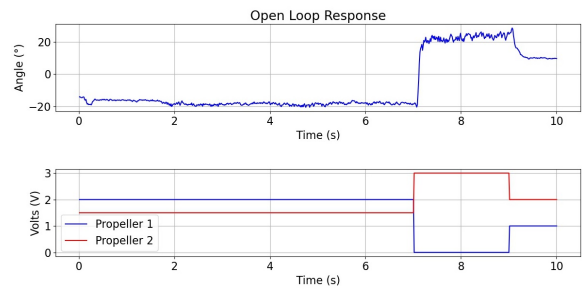


Fig. 6. Datalog used for identification

As can be seen in Figure 6, this sequence of steps applied at the input of the system, was chosen in such a way as to obtain the best multiple correction coefficient defined in (1)

$$\theta^T = [-1.057 \ 0.117 \ 0.144 \ -1.057 \ 0.332 \ 0.190] \quad (9)$$

Therefore, the system transfer function MISO $G(z)$ has been identified as

$$G(z) = \begin{bmatrix} G_1(z) \\ G_2(z) \end{bmatrix} = \begin{bmatrix} (0.144 - 1.057z^{-1})z^{-1} \\ 1 - 1.057z^{-1} + 0.117z^{-2} \\ (0.332 + 0.190z^{-1})z^{-1} \\ 1 - 1.057z^{-1} + 0.117z^{-2} \end{bmatrix} \quad (10)$$

In order to validate the estimated model, the same data set used to find the model was used in the validation, that way, the Figure 7 displays the measured signal (blue) and the estimated signal (red). It is observed that it was possible to make a good identification via NRLS, because for the same input signals applied in the identified model, the estimated signal responded very similarly to the read signal, in addition the multiple correlation coefficient obtained was $R^2 = 0.972$.

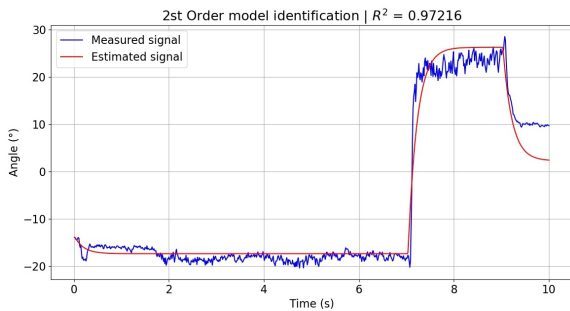


Fig. 7. Validation of the model estimated via non-recursive least squares in a polynomial approach.

3.2 NRLS: A state-space approach

In the previous subsection, the least squares estimator in a polynomial approach was presented, with the purpose of designing controllers that operate in a decentralized way. In this subsection, the NRLS estimator will be presented in a state space approach (SSLS) with the purpose of providing a model where the controller acts directly on the state variables in a centralized way. For this, we consider the model (ARX) represented in state space in Figure 8.

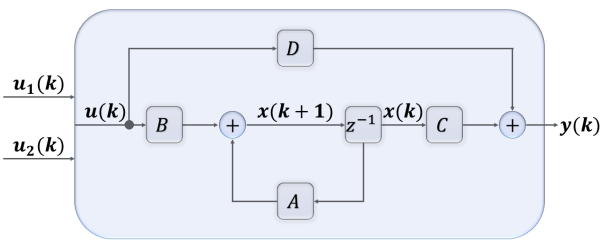


Fig. 8. Block diagram of system representation in state space

Considering the process as a second-order MISO model, the equation of states (11), and the output equation (12) can be represented as follows:

$$\begin{bmatrix} x_1(k+1) \\ x_2(k+1) \end{bmatrix} = \begin{bmatrix} a_{11} & a_{12} \\ a_{21} & a_{22} \end{bmatrix} \begin{bmatrix} x_1(k) \\ x_2(k) \end{bmatrix} + \begin{bmatrix} b_{11} & b_{12} \\ b_{21} & b_{22} \end{bmatrix} \begin{bmatrix} u_1(k) \\ u_2(k) \end{bmatrix} \quad (11)$$

$$y(k) = \begin{bmatrix} 1 & 0 \end{bmatrix} \begin{bmatrix} x_1(k) \\ x_2(k) \end{bmatrix} \quad (12)$$

Where $x_1(K)$ and $x_2(K)$ correspond to the angular position and angular velocity estimated, respectively. Thus, the SSLS solution lies in the determination of the estimated parameter vectors which is defined as (13)

$$\begin{bmatrix} \theta_1^T \\ \theta_2^T \end{bmatrix} = \begin{bmatrix} a_{11} & a_{12} & b_{11} & b_{12} \\ a_{21} & a_{22} & b_{21} & b_{22} \end{bmatrix} \quad (13)$$

For this, according to Silveira et al. (2020), it is necessary to use the calculation of future observations based on the vector of regressors, where, according to Nogueira et al. (2019), the estimation of the state x_2 is performed by means of an approximation of type *backward* of the derivative of x_1 . Thus, the state x_2 estimates the output speed x_1 as follows

$$x_2(k) = \frac{x_1(k) - x_1(k-1)}{T_s} \quad (14)$$

Thus, the matrix of regressors, for the SSLS case, is organized as in (15)

$$\phi = \begin{bmatrix} x_1(0) & x_2(0) & u_1(0) & u_2(0) \\ x_1(1) & x_2(1) & u_1(1) & u_2(1) \\ \vdots & \vdots & \vdots & \vdots \\ x_1(N-1) & x_2(N-1) & u_1(N-1) & u_2(N-1) \end{bmatrix} \quad (15)$$

Thus, the calculation of the estimated parameters, for the SSLS case, can be performed using (16)

$$\theta = (\phi^T \phi)^{-1} \phi^T \mathbf{y} \quad (16)$$

Where \mathbf{y} corresponds to the system output vector. From the input and output datalog in Figure 6, calculating (16), results in

$$\theta = \begin{bmatrix} 0.9452 & -4.0535 \\ 0.0016 & 0.1237 \\ -0.8370 & -62.0041 \\ 0.4805 & 35.5954 \end{bmatrix} \quad (17)$$

Therefore, the matrices A and B were calculated to be

$$A = \begin{bmatrix} 0.9452 & 0.0016 \\ -4.0535 & 0.1237 \end{bmatrix} \quad (18)$$

$$B = \begin{bmatrix} -0.8370 & 0.4805 \\ -62.0041 & 35.5954 \end{bmatrix} \quad (19)$$

To validate the model identified in state space, Figure 9 shows the read signal (blue) and the estimated signal (red), in this graph it is possible to verify that a good model was obtained, since the curves are similar. The multiple correlation coefficient obtained also indicates that the identified model is sufficiently well for practical applications, as the value obtained was $R^2 = 0.964$.

4. CONTROLLERS

Next, three types of digital controllers will be presented, of which the first controller, which is widely analyzed in

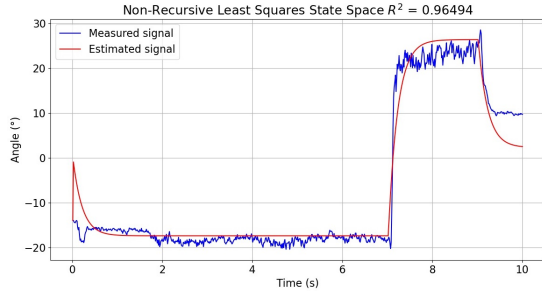


Fig. 9. Validation of the model estimated via non-recursive least squares in a state-space approach.

classical control theory, it's PID (Proportional + Integral + Derivative) controller. The second and third controllers analyzed in this article are optimal controllers, that is, according to Hespanha (2018), these methods consist in finding the control signal that minimizes a measure of output energy and energy consumption. These optimal controllers are strongly consolidated in modern control theory, thus generating great relevance in the aeronautical industry (Stevens et al., 2016).

In order to obtain a better visualization of the response curves in this article, the graphs analyzed later were plotted using the resource available on the HMI, which allows the user to plot and save the obtained graphs.

4.1 Proportional, Integral and Derivative (PID): Dynamic Cancellation

In summary, this tuning consists of canceling the plant's open-loop dynamics, imposing the desired first-order closed-loop dynamics, through an allocation of poles. For this, the controller tuning is done by choosing the closed-loop time constant τ_{cl} .

The development of the project and the control law for this controller is analogous to that described by Araujo et al. (2017), however, the system investigated in this work has two inputs ($u_1(k)$ and $u_2(k)$), and one output ($y(k)$), so the project applied to controller 1 is reproduced to controller 2 as shown in Figure 10.

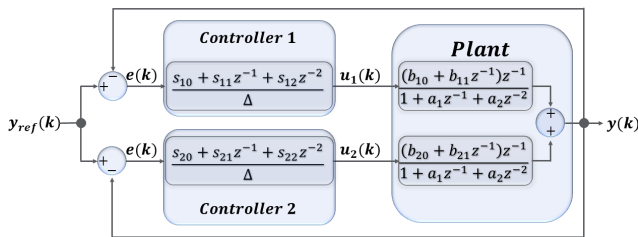


Fig. 10. System block diagram with PID controller via dynamic cancellation.

Thus, the control laws implemented were:

$$\begin{aligned} \Delta u_1(k) &= s_{10} + s_{11}z^{-1} + s_{12}z^{-2} \\ \Delta u_2(k) &= s_{20} + s_{21}z^{-1} + s_{22}z^{-2} \end{aligned} \quad (20)$$

Where s_{10} , s_{11} , and s_{12} are tuning parameters of controller 1, and s_{20} , s_{21} , and s_{22} are the parameters related to controller 2. These values can be calculated as follows:

$$\begin{aligned} z_{d1} &= e^{-\frac{T_s}{\tau_{cl1}}} \\ s_{10} &= \frac{1 - z_{d1}}{B_1(1)} \quad s_{11} = s_{10} \cdot a_1 \quad s_{12} = s_{10} \cdot a_2 \\ z_{d2} &= e^{-\frac{T_s}{\tau_{cl2}}} \\ s_{20} &= \frac{1 - z_{d2}}{B_2(1)} \quad s_{21} = s_{20} \cdot a_1 \quad s_{22} = s_{20} \cdot a_2 \end{aligned} \quad (21)$$

4.2 Linear Quadratic Regulator (LQR)

The controllers described above acted in the system, using descriptions by transfer functions, in a decentralized way. In this section, where the classical control theory includes the concepts of linear algebra, thus forming the modern control theory, the application of the LQR controller will be analyzed. In summary, this method is based on finding the optimal gain (K) of the controller, whose control law is given by:

$$u(k) = -Kx(k) \quad (22)$$

Which minimizes the discrete quadratic cost function:

$$J = \sum_0^{\infty} [x^T(k)Qx(k) + u^T(k)Ru(k)] \quad (23)$$

Where $x(k)$ are the state variables, Q is a positive-definite (or positive-semidefinite) Hermitian or real symmetric matrix and R is a positive-definite Hermitian or real symmetric matrix (Ogata, 2010). The solution of the optimization problem involving the equations (22) and (23), is obtained from the solution of the equation at differences of *Riccati* (*Recursive Riccati Difference Equation - RDE*) controller.

The plant used for this work is of type-0, so to be able to carry out the servo control, it was necessary to carry out an augmentation of states by adding an integrator Silveira et al. (2020). Thus, the new representation of the system, in state space, can be done as follows:

$$\begin{bmatrix} y(k) \\ \Delta x(k) \end{bmatrix} = \begin{bmatrix} I & CA \\ 0 & A \end{bmatrix} \begin{bmatrix} y(k-1) \\ \Delta x(k-1) \end{bmatrix} + \begin{bmatrix} CB \\ B \end{bmatrix} \Delta u(k-1) \quad (24)$$

$$y_a(k) = y(k) = [I \ 0] \begin{bmatrix} y(k) \\ \Delta x(k) \end{bmatrix} \quad (25)$$

After the augmentation of the model by the addition of an integrator, the *RDE* can be described by:

$$\begin{aligned} P(k+1) &= A_a^T P(k) A_a \\ &- A_a^T P(k) B_a (B_a^T P(k) B_a + R)^{-1} B_a^T P(k) A_a + Q \end{aligned} \quad (26)$$

The result of the controller *Riccati difference equation* is then used to calculate the optimal gain as follows:

$$K = [A_a^T P B_a (B_a^T P B_a + R)^{-1}]^T \quad (27)$$

Thus, the LQR control law for the augmented system is:

$$u_a(k) = \Delta u(k) = K [y_r(k) - x_a(k)]$$

$$u_a(k) = K \left\{ \begin{bmatrix} y_r(k) \\ 0 \end{bmatrix} - \begin{bmatrix} y(k) \\ \Delta x(k) \end{bmatrix} \right\} \quad (28)$$

5. RESULTS

4.3 Linear Quadratic Gaussian (LQG)

By the *separation principle* the regulator and the observer designs can be done separately, and then connect them (Stevens et al., 2016). From that, in this work, the LQG controller is implemented by joining the LQR project described in the previous section with a *Kalman Filter* (KF) (da Cruz, 1996), which will be described in this section.

The KF, being an optimal observer, is able to provide the controller with access to all state variables of the augmented model. Thus, the states of the identified model are optimally estimated by KF, which allows both measurement errors and modeling errors to be disregarded (Castro et al., 2020). For the implementation of KF with LQR, the following system described by the state space model is considered:

$$\begin{aligned} x(k+1) &= Ax(k) + Bu(k) \\ y(k) &= Cx(k) \end{aligned} \quad (29)$$

So, the KF problem can be summed up in obtaining the optimal gain of *Kalman*, such that the estimator given by

$$\begin{aligned} \hat{x}(k+1) &= A\hat{x}(k) + Bu(k) + L[y(k) - \hat{y}(k)] \\ \hat{y}(k) &= C\hat{x}(k) \end{aligned} \quad (30)$$

Be able to minimize the following estimation error

$$e_{est}(k) = x(k) - \hat{x}(k) \quad (31)$$

The calculation of L is based on the minimization of the quadratic functional

$$J = E \left\{ [x(k) - \hat{x}(k)]^T [x(k) - \hat{x}(k)] \right\} \quad (32)$$

The calculation of the optimal gain of *Kalman* (L) can be done analogously to the calculation of the optimal controller gain (LQR), since both the regulation and observation problems they are dual. Thus, knowing that the system was augmented by the inclusion of an integrator, the covariance matrix, which is calculated from the *Riccati difference equation* of the estimator, can be calculated as in (33)

$$\begin{aligned} S(k+1) &= A_a S(k) A_a^T \\ &- A_a S(k) C_a^T (C_a S(k) C_a^T + R_{kf})^{-1} C_a S(k) A_a^T \\ &+ Q_{kf} \end{aligned} \quad (33)$$

The result of (33), is then used to calculate the optimal gain as follows

$$L = A_a S C_a^T (C_a S C_a^T + R_{kf})^{-1} \quad (34)$$

All controllers below were tuned in such a way that the closed-loop response resulted in a signal with a stabilization period less than or equal to two seconds ($t_s \leq 2s$) and a overshoot less than or equal to ten percent of its value in steady state ($M_p \leq 10\%$).

5.1 Proportional, Integral and Derivative (PID): Dynamic Cancellation

This time, to achieve the performance specifications $t_s \leq 2s$ and $M_p \leq 10\%$, the value used to tune both controllers was $\tau_{cl1} = \tau_{cl2} = 1s$, thus generating the control laws:

$$\begin{aligned} \Delta u_1(k) &= -0.0243 + 0.0257z^{-1} - 0.0028z^{-2} \\ \Delta u_2(k) &= 0.0424 - 0.0449z^{-1} + 0.0050z^{-2} \end{aligned}$$

As can be seen in Figure 11, the dynamics obtained in closed loop corresponded as expected using the tuning $\tau_{cl1} = \tau_{cl2} = 1s$.

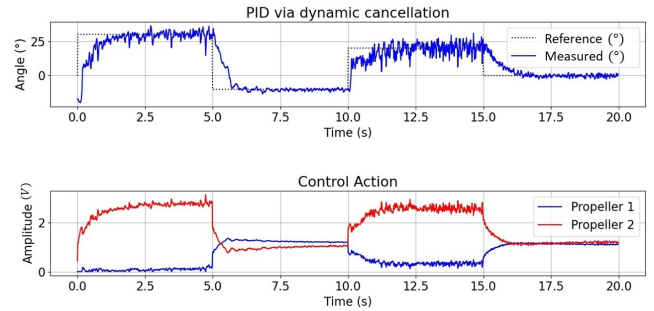


Fig. 11. System response to PID controller via dynamic cancellation.

5.2 Linear Quadratic Regulator (LQR)

For the LQR tuning, the following covariance matrices were used:

$$Q_{lqr} = \begin{bmatrix} 1 & 0 & 0 \\ 0 & 10 & 0 \\ 0 & 0 & 1 \end{bmatrix} \quad e \quad R_{lqr} = \begin{bmatrix} 20000 & 0 \\ 0 & 20000 \end{bmatrix} \quad (35)$$

What resulted in the covariance matrix (36) and the optimal gains matrix (37):

$$P = \begin{bmatrix} 19.9144 & 136.5467 & 0.2095 \\ 136.5467 & 1643.5427 & 2.0485 \\ 0.2095 & 2.0485 & 1.0160 \end{bmatrix} \quad (36)$$

$$K = \begin{bmatrix} -0.0052 & -0.0513 & -0.0004 \\ 0.0030 & 0.0294 & 0.0002 \end{bmatrix} \quad (37)$$

Therefore, the controller control law LQR for this MISO system was as follows:

$$\Delta u(k) = -Kx_a(k) + K_y y_r(k)$$

$$\Delta u(k) = - \begin{bmatrix} -0.0052 & -0.0513 & -0.0004 \\ 0.0030 & 0.0294 & 0.0002 \end{bmatrix} \begin{bmatrix} y(k) \\ \Delta x(k) \end{bmatrix} + \begin{bmatrix} -0.0052 \\ 0.0030 \end{bmatrix} y_r(k) \quad (38)$$

Where the first installment of the (38) corresponds to the regulatory case, and the second to the servo case. Figure 12 shows the response of LQR to the tuning used in (35):

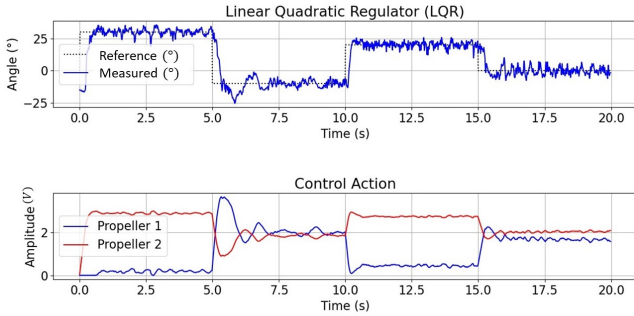


Fig. 12. System response to controller LQR

5.3 Linear Quadratic Gaussian (LQG)

For the LQR tuning, the following covariance matrices were used:

$$Q_{lqr} = \begin{bmatrix} 1 & 0 & 0 \\ 0 & 10 & 0 \\ 0 & 0 & 1 \end{bmatrix} \text{ e } R_{lqr} = \begin{bmatrix} 10 & 0 \\ 0 & 10 \end{bmatrix} \quad (39)$$

And for KF tuning, knowing that the smaller the value of a given diagonal element of Q_{kf} , the more its corresponding state variable (Stevens et al., 2016) is filtered, and that the matrix R_{kf} is responsible for shifting the magnitude-to-frequency curve sideways. The tuning used to estimate the states were

$$Q_{kf} = \begin{bmatrix} 10^{-6} & 0 & 0 \\ 0 & 1 & 1 \\ 0 & 0 & 1 \end{bmatrix} \Big| R_{kf} = 10.10^3 \quad (40)$$

What resulted in the covariance matrix (41) and the optimal gains matrix (42)

$$S = \begin{bmatrix} 932.7802 & 42.8556 & -212.8282 \\ 42.8556 & 7.1268 & -29.8321 \\ -212.8282 & -29.8321 & 146.6314 \end{bmatrix} \quad (41)$$

$$L = [0.0889 \ 0.0036 \ -0.0182] \quad (42)$$

5.4 Performance indices

In order to compare the effectiveness of the controllers, the following performance indices were used: integral square error (ISE), integral squared control signal (ISU), $ISE + ISU$, error variance σ_e^2 , and control signal variance σ_u^2 , these metrics were calculated this way:

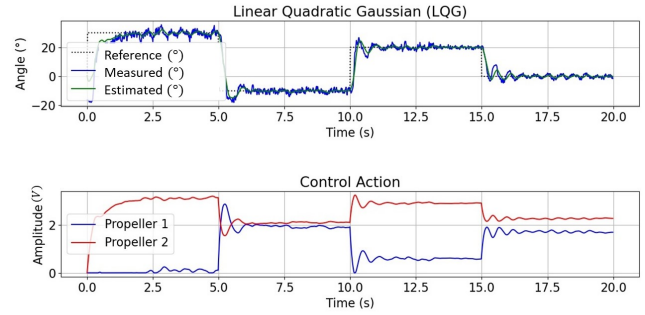


Fig. 13. System response to controller LQG.

$$\begin{aligned} ISE &= \frac{1}{N} \sum_{k=1}^N [y_r(k) - y(k)]^2 \\ ISU &= \frac{1}{N} \left\{ \sum_{k=1}^N [u_1(k)]^2 + \sum_{k=1}^N [u_2(k)]^2 \right\} \\ \sigma_e^2 &= \frac{1}{N} \sum_{k=1}^N [e(k) - \mu_e]^2 \\ \sigma_u^2 &= \frac{1}{N} \left\{ \sum_{k=1}^N [u_1(k) - \mu_{u_1}]^2 + \sum_{k=1}^N [u_2(k) - \mu_{u_2}]^2 \right\} \end{aligned} \quad (43)$$

Where N , y_r , y , u_1 , u_2 , μ_e , μ_{u_1} , μ_{u_2} correspond to the number of samples, angle of reference, measured angle, controller 1 signal, controller 2 signal, mean error value, mean value of controller 1 signal, and mean value of controller 2 signal, respectively. The tables 1 and 2 present the comparisons between the indices related to the cost function and the indices related to the variances, respectively:

Table 1. Comparison among indices related to the cost function

	ISE	ISU	ISE+ISU
PID	76.615	4.563	81.178
LQR	59.993	7.828	67.820
LQG	57.186	8.421	65.607

Table 2. Comparison between indices related to variance

	σ_e^2	σ_u^2
PID	76.335	0.838
LQR	59.771	1.082
LQG	56.373	0.789

6. CONCLUSIONS

Through the values presented in Table 1, it is possible to see that the best controller, in terms of energy consumption for this process, was the PID, as it was the one that acted generating the lowest ISU. On the other hand, the controller that acted with the smallest reference tracking error (smallest ISE), and provided the best cost of efficiency ($ISE + ISU$), was LQG. For situations where high pitch variances are not desired, the Table 2 indicates that the controller that performed better was the LQG,

and for situations where they are not desired high variances of the signal injected into the motors, the controller that performed best was the LQG, since the *Kalman* filter reduces measurement noise.

REFERENCES

- Aguirre, L.A. (2014). *Introdução à identificação de sistemas—Técnicas lineares e não-lineares aplicadas a sistemas reais*. Editora UFMG, Belo Horizonte.
- Araujo, M.S., Dutra, Bruno G. and Pinheiro, T.C.F., Cunha, L.B., and Silveira, A.d.S. (2017). Projeto de controladores digitais pid e i-pd via rst: Uma análise de desempenho. In *Simpósio Brasileiro de Automação Inteligente (SBAI)*.
- Castro, L., Cunha, L., Dutra, B., and Silveira, A. (2020). Digital lqg controller design applied to an electronic system. *IEEE Latin America Transactions*, 18(03), 581–588.
- Coelho, A.A.R. and dos Santos Coelho, L. (2016). *Identificação de sistemas dinâmicos lineares*. editora ufsc, Florianópolis: Ed. da UFSC.
- da Cruz, J.J. (1996). *Controle Robusto Multivariável: O Método LGQ/LTR Vol. 05*. EdUSP.
- Friedland, B. (2012). *Control system design: an introduction to state-space methods*. Courier Corporation.
- Hespanha, J.P. (2018). *Linear systems theory*. Princeton university press.
- Misgeld, B.J., Pomprapa, A., and Leonhardt, S. (2013). Didactic approach to multivariable control using iec 61131 model-based design and programmable logic controllers. *IFAC Proceedings Volumes*, 46(17), 220–225.
- Nogueira, C.E.D., Silveira, A.d.S., Yamaguti, N.N.N., and Sodr , L.d.C. (2019). Desenvolvimento e identifica o de uma planta mimo de duas entradas e duas saídas para ensino de sistemas de controle. *cobenge*.
- Ogata, K. (2010). *Modern control engineering*. Prentice hall.
- Silveira, A., Silva, A., Coelho, A., Real, J., and Silva, O. (2020). Design and real-time implementation of a wireless autopilot using multivariable predictive generalized minimum variance control in the state-space. *Aerospace Science and Technology*, 105, 106053.
- Stevens, B.L., Lewis, F.L., and Johnson, E.N. (2016). *Aircraft control and simulation: dynamics, controls design, and autonomous systems*. John Wiley & Sons.
- Yip, L.C. (1984). Vstar ch-47b: A variable-stability research helicopter. *NASA AMES SUMMER HIGH SCHOOL APPRENTICESHIP RESEARCH PROGRAM*, 133.